Atmos. Chem. Phys. Discuss., https://doi.org/10.5194/acp-2019-399
Manuscript under review for journal Atmos. Chem. Phys.
Discussion started: 20 May 2019

The roles of island size and orography on tropical convection and aerosol transport

Stacey Kawecki
Colorado State University

Susan van den Heever
Colorado State University

Abstract

This study investigates the impact of island diameter size and orographic height on precipitation, convective organization and aerosol transport on and around tropical islands. Twenty-four model simulations are set up and run, in which the island diameter (50 km, 100 km, and 200 km) and peak orographic height (flat, 500 m, 1 km, and 2 km) are independently and simultaneously varied under weak and strong zonal wind regimes. In these simulations, unlike many of the previous island flow investigations, the full three-dimensional flow over and around islands is resolved. Analysis of these numerical experiments demonstrates that island orographic height is a stronger control than island size on precipitation, convective organization, and aerosol redistribution. The wind regime is found to modulate these results. Under the strong zonal wind regime, increasing orographic height induces changes to the flow around the island, leading to lee-vortex formation, reverse flow, and the earlier development of deep convection than in the flat simulation. In the weaker zonal wind experiment, increasing orographic height enhances the role of radiational heating, leading to enhanced upslope flow and stronger convergence, which produces earlier deep convection than in the flat simulation. The timing and location of the sea breeze/mountain breeze convergence determines the location of the initial vertical aerosol mixing with cloud formation and entrainment, whereas the timing of deep convection formation dictates how quickly the aerosols are mixed out of the boundary layer. Finally, it is demonstrated that cold pools play an important role in the propagation of convection towards the shore in the simulations with orography.

1.0 Introduction

Coastal regions are attractive places to live for numerous reasons including health and recreational benefits. Sea ports and harbors also play an important role in the global economy and transportation industry. Approximately 10% of the global population lives in low-elevation coastal zones (McGranahan et al., 2007), and it is projected that the population density within these regions will continue to grow throughout the next century (Neumann et al., 2015). Any changes to the meteorology, air quality and visibility of these regions will therefore affect a substantial portion of the population and its livelihood.

The considerable uncertainty surrounding aerosol effects on clouds and climate (Boucher et al., 2013; Tao et al., 2012) extends to aerosol transport within coastal and island regions. Furthermore, the meteorology and associated air quality and visibility within coastal regions are frequently governed by local-scale thermally-induced circulations, such as land and sea breezes and mountain-slope flows for land masses with near-coastal topography. In spite of their importance to human health and safety, these coastal circulations are often poorly represented in models, from climate models to regional and weather prediction models (Birch et al., 2015), which makes the accurate prediction of these features challenging. Furthermore, mountainous islands can exert a significant impact on the large-scale dynamics through drag (McFarlane, 1987), and yet are often too small to be resolved in global models (Glover, 1999; Neal and Slingo, 2003). Efforts are currently underway to parameterize these effects (Choi and Hong, 2015). To effectively parameterize these processes, we need to enhance our understanding of the roles played by mesoscale coastal circulations, such as land and sea breezes, on the distribution of coastal aerosols, as well as the impacts of local environmental conditions including precipitation and convective processes, on this aerosol transport.

The land and sea breeze circulation is driven by differential heating over land and ocean that results in a baroclinic circulation (Pielke, 1974; Mahrer et al., 1977; Baker et al., 2001). This circulation is induced when the differential heating of the ocean and adjacent land causes a tilt in the isobaric and isopycnal surfaces over the land-sea interface. The intersection of the tilted pressure and density surface induces the circulation from ocean to land during the day (Holton, 2012). At night, the circulation is reversed because the land surfaces cool more rapidly than the ocean. Anabatic and katabatic winds are mountain-plains circulations that also occur due to the differential heating and cooling of mountain slopes and the surrounding plains, leading to upslope flow during the day and downslope flow at night. On mountainous islands, the sea breeze and the mountain breeze can interact with each other, thereby impacting convergence and associated convection (Wang et al., 2017). Wang and Kirschbaum (2017) investigated the influence that mountain height has on the sea breeze and mountain-plains solenoid circulation using a suite of numerical simulations. They found that with quiescent initial conditions, increasing orographic height eventually decreases the strength of the sea breeze front. The daytime upslope flow from the mountain warming draws the pre-sea-breeze frontal air upslope, thereby weakening the convergence that would typically occur at the sea breeze front, as the mass ahead of the front is moving away from, rather than towards, the front.

Convection and precipitation on and around islands have also been investigated as a function of island size and background winds using the Tropical Rainfall Measuring Mission (TRMM), idealized modeling, and a satellite simulator (Robinson et al., 2011). Robinson et al (2011) defined convective vigor as stronger precipitation rates and higher cloud top heights. They found from their study that convective vigor systematically increased with increasing island size in several different convective environments in which the relative humidity and wind shear were altered. The presence of a strong background wind has also been found to increase precipitation amounts on the windward side of islands, and increasing the orographic height of the island was associated with an increase in windward precipitation amounts (Wang and Sobel, 2017). In the tropical Atlantic, the trade winds encountering mountainous islands have also been found to mechanically force convection as air travels up and over the mountains, subsequently increasing the windward precipitation, (Nugent et al., 2013). Also, the formation of vortex pairs in the lee of islands can contribute to the initiation of convection (Smolarkiewicz et al., 1989).

While our understanding of the impacts of island flow regimes on convection and precipitation has been significantly enhanced by these previous idealized modeling studies, a number of them have been based on simulations using simplified representations of island morphology and characteristics. "Gaussian strip" islands have been implemented in which the zonal mountain profile is prescribed with a Gaussian curve (unvarying in the meridional direction), and the horizontal area of the island is represented by a rectangle that extends the entire length of the meridional dimension of the model domain. While this type of idealized configuration has often been used to great effect (Robinson and Sherwood, 2011; Nugent and Minder, 2013; Wang and Kirchbaum, 2017; Wang and Sobel, 2017), it may have unintended shortfalls when considering the three-dimensional wind flow and associated mass transport *around* islands in that "strip" islands do not allow for flow to divert around the obstacle. The absence of the around island flow may also have implications for flow that is blocked, either partially or fully, by topography, and hence on convective initiation and precipitation accumulation. The land surface assumptions of these "strip" islands is also quite often simplified. For example, Robinson et al (2011) made use of water as their lower boundary condition, and land was mimicked by disabling the latent heat fluxes and increasing the radiative fluxes in the region of the strip. Aspects such as differential surface roughness lengths, latent heat fluxes and surface friction are also quite often excluded (Robinson and Sherwood, 2011). The research presented in this paper will build on and extend these prior studies through the use of simulations that include three-dimensional, circular, mountainous islands and a fully interactive surface scheme.

To address the difficulties in forecasting and observing three-dimensional aerosol distribution and visibility in the littoral zones, a holistic approach involving a large team of scientists utilizing process-based modeling, satellite observations and data assimilation has been undertaken in the Office of Naval Research (ONR)-supported Holistic Analysis of Aerosols in Littoral Environments (HAALE) Multidisciplinary University Research Initiative (MURI). Such a holistic approach is necessary in order to draw on the complementary strengths of each methodology. For example, while the characteristics and transport of aerosols are often detected and successfully analyzed through the use of remote sensing platforms, such approaches are complicated within coastal regions by the high spatio-temporal heterogeneity of water turbidity, tidal influences, and complex coastlines (Kanitz et al., 2014). Combining the satellite and modeling platforms through the use of tools such as satellite simulators, the physical processes that govern aerosol transport in such heterogeneous environments can be investigated, and this new knowledge can then be applied to aspects such as retrieval algorithms and parameterization development.

The research outlined in this paper contributes to the ONR MURI effort by addressing the following question: "How do island size and orography affect convective organization, precipitation and aerosol distributions within tropical maritime environments?" More specifically, the goal of this study is to understand how island size and topographic height influence flow over and around three-dimensional islands and the subsequent impacts on convective cloud systems and aerosol transport. The suite of numerical experiments used to achieve this goal are described in Section 2. A discussion of the experiment results occurs in section 3 and the implications of these results and conclusions are presented in section 4.

2.0 Model Setup and Experimental Design

Twenty-four simulations are performed using the open source Regional Atmospheric Modeling System (RAMS: Pielke et al., 1992; Saleeby and van den Heever, 2013), version 6.2.05 in an idealized setting. RAMS includes sophisticated microphysical (Saleeby et al., 2004; Saleeby et al., 2008), land surface (Walko et al., 2000b) and tracer parameterizations, all of which are necessary to conduct the proposed research. The microphysical parameterization is a two-moment, bin-emulating scheme (Saleeby and Cotton 2004) and tracks microphysical and aerosol process information at all timesteps throughout the domain (Saleeby and van den Heever 2013). The RAMS model allows the user to methodically specify and vary the inputs. For example, the user can build a model domain surface that consists of a circular and mountainous island that is surrounded by ocean, where the ocean surface and island surface have specific roughness lengths and emissivities. This means that for simulations utilizing identical atmospheric conditions over the land and ocean that the respective surface fluxes and friction-induced convergence will differ. Table 1 summarizes the model simulation configurations and parameterizations used for this investigation.

To test the effects of island size on the flow around three-dimensional islands, we start with circular islands with three different diameters: 50km, 100km, and 200km. The experimental setup is shown in Table 2. The horizontal model domain size is varied with island size in order to ensure that the land to ocean ratios are similar, and hence that each island has similar amounts of water vapor available for convective processes. Domain sizes of 100km x 100km, 200km x 200km and 400km x 400km are used for the 50 km, 100 km and 200km diameter islands, respectively. The lateral boundary conditions are cyclic. The number of vertical levels is constant for all simulations, with 200 levels at 100 m grid spacing. The model top reaches 20 km AGL. All of the simulations utilize a horizontal grid spacing of 1-km. The horizontal and vertical grid spacing mimic the grid set up from Robinson et. al (2011), thereby facilitating comparisons.

Sensitivity tests with orography use the "Witch of Agnesi" mountain and four peak orographic heights are tested: flat, 500 meters, 1 kilometer, and 2 kilometers (Figure 1a; Table 2). Mountain half-widths vary with island size, but not with peak orographic height and are 12 km for the 50-km diameter islands, 25 km for the 100 km islands, and 50 km for the 200 km islands. Therefore, for a given island diameter, the orographic slopes increase with increasing orographic height. Figure 1a demonstrates the topography and domain setup for the 100-km diameter, 1-km orography simulation. Each simulation is run for one full diurnal cycle and does not include the Coriolis effect.

This suite of 12 simulations testing island size and orographic height (Table 2) is initialized with two different soundings. These two soundings are representative of typical tropical maritime convective regimes and are utilized in order to further understand the role that background winds play in convective organization and tracer redistribution (Figure 1b). They are taken from the group of six soundings used by Robinson et al (2011), which were formulated from 405 NCEP reanalysis soundings taken from January 1998 through December 2007 in order to correspond to the TRMM data they analyzed. To test the effects that different wind regimes have on island flows and aerosol redistribution, soundings with a strong zonal wind (STRONG-EXP) and a weak zonal wind (WEAK-EXP) are selected for model initialization. All of the simulations are initialized horizontally homogeneously using the selected soundings. Evergreen shrub was specified as the land surface vegetation, and the surrounding oceans have a fixed SST of 293 K.

To gauge the aerosol redistribution that occurs as a function of island size, orography and wind regime, eight different tracers are released within 4 vertical levels, one in each level over land and one in each of the 4 corresponding levels over ocean. The levels are as follows: 0-500 m above ground level (AGL), 500-1000 m AGL, 1000-1500 AGL, and 1500-2000 AGL (Figure

1c). These eight distinct tracers are tracked throughout the model domain at every time step. Using the tracers as proxies for aerosols, the tracer placement allows for the assessment of the predominant altitudes from which aerosols are entrained into the convection and / or lofted over and around the islands. The tracers are released at the beginning of the simulation with a concentration of 1 kg tracer/kg air and are passive in that they are not microphysically nor radiatively active, however they are advected around the domain by the three-dimensional wind field and thus are most suitable for the goals of this research.

3.0 Results

In the following sections, flow regimes, convective intensity metrics, precipitation, and the tracer redistribution are all examined in order to understand the influence that island size, island orographic height, and background winds have on convective organization and tracer redistribution.

3.1 Flow Fields and Moisture Convergence

Orography is known to substantially alter the wind flow over mountainous terrain via dynamical and / or thermo-dynamical forcing (Chen et al., 1994; Houze, 2012). In order to examine the influence that island orography and island size have on convective organization, precipitation accumulation, and aerosol redistribution, we must first determine how changes to these factors alter the flow over and around the island.

3.1.1 Surface Streamlines

The WEAK-EXP and STRONG-EXP surface streamlines are examined at 08:30 UTC (Figure 2). This time is selected as it falls after sunrise but before deep convection initiates, which substantially alters the surface winds. As our analysis below demonstrates that island orography has a stronger influence than island size on the flow regime, only the results from the

100-km diameter island simulations are shown here. Furthermore, in the interest of brevity, just the flat and 1-km simulation results are discussed. However, the trends are consistent across both island size and orography. It should also be noted that the background flow in the STRONG-EXP and WEAK-EXP are westerly and northwesterly, respectively (Figure 1b).

The STRONG-EXP flat simulation (Figure 2a) clearly shows that the zonal flow is only weakly altered by the presence of the island, with some convergence of the flow on the lee side of the island. Over the island, the surface roughness is greater than that over the ocean, which increases the frictional drag, thus slowing the flow and producing the observed convergence. Downwind of the island, the reduced frictional drag over the ocean produces divergence of the flow, a drop in the low-level pressure, and a corresponding turn of the downstream flow towards the lower pressure. The 1-km STRONG-EXP simulation (Figure 2b), in which the 1km orography has been incorporated, has considerably different flow features at the same point in time. First, a strong reversal of the flow develops in the lee of the mountain (Figure 2b, black triangle). The reverse flow occurs as a result of lee-vortex formation, a phenomenon that has both been previously observed (Smith et al., 1993) and modeled (Smolakareic and Rotunno, 1989) for Froude numbers ranging from 0.1-0.5. The streamlines do show the flow going around the island, which aids in the formation of the lee vortices (Figure 2b, black 'X') that then assist in driving the reverse flow (Smolakareic and Rotunno, 1989). This reverse flow then meets the over-the-mountain flow at the stagnation point (Figure 2b, black diamond).

To compare our simulations with previous work, we calculate the dimensionless Froude number (1) at the model initialization for each grid point for each simulation, where $\mathbf{U}$ (m s^{-1}) is the u-component of the wind, $\mathbf{N}$ (s^{-1}) is the Brunt-Vaisala frequency (2) and $\mathbf{h}_m$ is the height of the obstacle in meters. For the Brunt-Vaisala frequency, $\mathbf{g}$ is gravity (9.8 m s^{-2}), $\boldsymbol{\theta}_o$ is the lowest model level potential temperature (K), and $\partial\boldsymbol{\theta}/\partial\mathbf{z}$ is calculated from the model grid.

Atmos. Chem. Phys. Discuss., https://doi.org/10.5194/acp-2019-399
Manuscript under review for journal Atmos. Chem. Phys.
Discussion started: 20 May 2019

$$Fr = U/h_m * N \qquad [1]$$

$$N = \sqrt{\left[\frac{g}{\theta o}\frac{\partial\theta}{\partial z}\right]} \qquad [2]$$

Because of the wind shear in the simulations, only the first 30 model levels (lowest 3 km) are used in the calculation. To attain one value for each simulation, the Froude number values for each model grid cell were averaged over both the lowest 30 model levels and the entire horizontal extent of the domain(s). The Froude number for the STRONG-EXP 1-km simulation is 0.04, about one order of magnitude smaller than the conditions utilized in previous modeling work that exhibit critical or supercritical flows (Smolakareic and Rotunno, 1989; Wang and Sobel, 2017). The STRONG-EXP simulations, while having a relatively low Froude number, exhibits characteristics of critical flows, such as a wake and lee vortex formation. In the WEAK-EXP flat simulation (Figure 2c), the streamlines originate from the northwest and weakly converge in the lee of the island. However, the 1-km WEAK-EXP simulation conveys a different flow regime (Figure 2d). The WEAK-EXP has a Froude number of 0.01, which is characteristic of tranquil flow. Under such conditions diurnal heating can more easily influence local circulations than with stronger, more turbulent flows evident in the STRONG-EXP 1-km simulation. At 08:30 UTC, upslope flow exists symmetrically around the entire island, which is characteristic of daytime mountain circulations, and hence of the role of diurnal heating.

Finally, after deep convection is initiated in all simulations, these early morning initial flow features break down (not shown) in all of the STRONG-EXP and WEAK-EXP simulations.

3.3.2 Moisture Flux Divergence

The moisture divergence field conveys how the island-altered flow redistributes the water vapor near the surface, and thus how the three basic ingredients for convection, moisture, instability, and lift (Emmanuel, 1994), are altered. To obtain the near-surface three-dimensional moisture flux divergence field, the lowest model level above the model ground was used (Figure 3). A snapshot at 08:30 UTC is examined to relate the streamlines to the moisture field shown above. At 08:30 UTC in the STRONG-EXP Flat simulation (Figure 3a), the region of strongest moisture convergence unsurprisingly corresponds to the regions where the streamlines are diverted inwards towards the island, as described in the previous section. In the WEAK-EXP flat simulation (Figure 3c), the region of moisture flux convergence circumnavigates the island almost symmetrically and is reflective of the inland propagation of the sea breeze. In the WEAK-EXP, where the background winds are weaker than in the STRONG-EXP, the sea breeze circulation dominates the near-surface moisture flux distribution. In the STRONG-EXP 1-km simulation, the predominant moisture convergence is coincident with the stagnation point (Figure 3b, black diamond) and subsequent vortex and wake formation (Figure 3b, 2b, black triangle). These regions of moisture flux convergence indicate those regions that deep convection is more likely to initiate and will also impact convective organization. Finally, in the WEAK-EXP 1-km simulation, moisture flux divergence occurs within the upslope flow (Figure 3d, black circles) ultimately culminating in moisture flux convergence at the top of the island. A region of moisture flux convergence also develops where the upslope flow interacts with the background flow on the western side of the island (Figure 3d, black star). These regions of moisture flux convergence are early indicators of where clouds are most likely to develop as they are associated with both low-level convergence and enhanced moisture availability.

In summary, in the flat island cases there are zones of enhanced moisture convergence, and thus potential connective initiation, near the island edges. However, with the addition of topography, the moisture flux convergence shifts towards the mountain tops in the WEAK-EXP cases and to the lee in the STRONG-EXP cases. These topographically-induced shifts govern where convective initiation is most likely to occur.

3.2. Convective Organization and Intensity

As was shown in the previous section, increasing the topography of a circular island substantially alters the flow and the moisture flux convergence around the island. It follows that these flow changes can affect the organization and intensity of the convection that develops. In this section, metrics of convective intensity and organization are examined to understand how the changes in the flow regime can alter the character of deep convection.

3.2.1 Cloud top height

Cloud top height is frequently used as a proxy for convective intensity (Adler et al, 1986; Sherwood et al 2004) as this variable is indicative of updraft strength and hence as to how deep the convection becomes. Figure 4 is a Hovmoller diagram of latitudinally averaged cloud top height, with time ranging from 06:00 – 16:20 UTC on the ordinate axis, and the averaged latitudinal value along the abscissa. Due to the use of the cyclic boundary conditions, the convective features from the eastern boundary do begin to affect the incoming/western boundaries after 1620 UTC, and the analysis is therefore terminated at that time. The STRONG-EXP (Figure 4 a-d) and WEAK-EXP (Figure 4 e-h) simulations demonstrate similar trends in the orographic influence on convective storm development. The flat topography simulations (Figure 4a and d) are characterized by shallow convection over the island early (9:00 UTC). The cloud top heights increase vertically, expand horizontally and ultimately converge in the island center at ~12:00 UTC. This phenomenon is more obvious in the STRONG-EXP flat simulation, but also exists in the WEAK-EXP flat simulation. Including topography changes this behavior of this convective organization. In the STRONG-EXP, increasing orographic height to only 500 meters causes a substantial change in the character of convection (Figure 4b). Instead of convection beginning within shallow clouds systems and converging towards the island center as in the flat case, convection begins earlier (08:30 UTC) near the center of the island, and subsequently expands towards the shore with time (Figure 4b). The speed of the shoreward expansion increases with increasing orographic height (Figures 4c-d). While increasing the topographic height to 1 km AGL increases the occurrence of 13 km cloud top heights, further increasing the orographic height to 2 km does not have the same result (Figure 4d). The deepest convection is still generally concentrated in the middle of the island, with cloud tops exceeding 13 km, however, the contiguous area of cloud top heights greater than 13 km is smaller in the 2-km topography simulation than in the 1-km topographic simulation, in spite of the more rapid expansion towards the shore in this simulation.

Enhancing the orography in the WEAK-EXP simulations also changes the behavior of the convection development and organization. However, the change in convective behavior in the WEAK-EXP simulations does not appear to be as extensive as in the STRONG-EXP simulations. In the 500-m orographic height simulation, the initial convection is shallow and scattered, but it is not until 12:00 UTC that the cloud top heights become higher, although the cloud coverage is more contiguous in the 500-m simulation (Figure 4f) than in the flat simulation (Figure 4e). The change in the timing of convection becomes more apparent when the orographic height is increased to 1 km (Figure 4g). In this simulation, the evolution of cloud top height begins to more closely resemble the STRONG-EXP orographic simulations. Convection begins near the island center and expands horizontally and vertically, reaching up to 11 km AGL in height in most of the convective region, and expanding towards the shore from 11:00-12:00 UTC. The 2-km WEAK-EXP simulation looks the most like the STRONG-EXP orographic simulations, with deep convective triggering at the center of the island and convective cloud tops reaching over 13 km at 09:00 UTC (Figure 4h), and subsequently expanding towards the shore at a rate similar to the 1-km STRONG-EXP.

Overall, increasing the orographic height changes the distribution and organization of convection regardless of the wind regime. In the flat topography simulations, convection begins as scattered, low-level cumulus clouds that grow upscale, developing progressively towards the center of the island. However, with increasing orography, deep convection initiates near the island center and then radially expands towards the shoreline.

While deep convection initiates near the island center in both the WEAK-EXP and STRONG-EXP with high topography, the processes that produce this deep convective initiation vary as a function of wind regime. In the STRONG-EXP simulations, the lee vortex pair development and strong reverse flow associated with the increased orography (Figures 1 and 2) increases surface moisture flux convergence (Figure 3) near the stagnation point on the lee side of the island, which leads to the earlier development of deeper convection. However, in the WEAK-EXP experiments, the thermally induced upslope flow creates moisture flux convergence near the mountain top, which then initiates deep convection in the island center, followed by the expansion of this cloud development towards the coast.

3.2.2 Cloud water mixing ratios

Another metric that is often used to examine convective organization is the cloud water mixing ratio distribution as represented through contour frequency with altitude diagrams (CFADs) (Yuter and Houze, 2005) (Figure 5). Cloud water mixing ratios over land are considered for the period 0600-1620 UTC, which is the same period as the cloud top height hovmoller plots. As with the cloud top height analysis, increasing orographic height substantially alters the distributions of cloud water mixing ratio. In the STRONG-EXP flat simulation (Figure 5a), there is a bimodal distribution of the cloud water mixing ratio, with peaks in the boundary layer and upper levels. The boundary layer peak is representative of the shallow cumulus convection that develops in response to the sea-breeze driven ring of moisture flux convergence near the coastline (Figure 2a). The second peak is evident at altitudes ranging from 10 km to 15 km. Compared to the boundary layer peak, this second peak has a wider cloud water distribution at higher altitudes. This is indicative of the convection that grows upscale in the flat simulation. Increasing the orographic height to 500 meters changes the cloud water distribution, both in terms of the altitude of where clouds occur, as well as the mixing ratio magnitudes (Figure 5b). The frequency of the shallow convective mode decreases, and the deep convective mode peaks at 14 km. Increasing orography to 1 km further diminishes the probability of shallow convection (Figure 5c), while enhancing the likelihood of deep convection. Increasing the orographic height therefore appears to increase the probability of higher clouds with greater water contents and reduces the probability of shallow cumulus convection.

In the WEAK-EXP simulations, shallow convection gradually gives way to deeper convection with increasing orographic height (Figure 5e-h). The deep convection is generally shallower than the deep convection that is observed in the corresponding STRONG-EXPs, and the cloud mixing ratios also tend to be less. Furthermore, in the WEAK-EXP simulations, the bimodal distribution cloud water distribution requires an increase to 2 km orography before only a single mode of convection is evident. The shallow clouds that occur in both the STRONG-EXP and WEAK-EXP are associated with the early moisture flux convergence near the surface. In the STRONG-EXP, this is comprised of the shallow clouds forming on the windward side of the island in association with the more pronounced inland propagation of the sea breeze due to the stronger background winds. In the WEAK-EXP, the ring of clouds forming around the entire island in association with the symmetrically developing sea breeze comprises the shallow mode.

3.2.3 Cold pools

In this section, the mechanisms behind the change from inland expansion and vertical growth of convection to the shoreward propagation of convection with increasing orographic height is assessed. First, the influence of cold pools on the development and propagation of convection towards the shore is examined. Snapshots representing the temporal progression of the near-surface perturbation potential temperature, surface winds, and the vertically-integrated condensate are shown in Figure 6. The perturbation potential temperature has been calculated by taking the difference of the potential temperature from the average potential temperature over the entire lowest model level at that time, including both the ocean and the land portions of the domain.

The WEAK-EXP flat simulation at 06:00 UTC (Figure 6a), demonstrates the environmental state before sunrise, where the perturbation potential temperature is approximately constant across the domain, and the flow is laminar and from the north northwest (Figure 6a). By 09:30 UTC in the flat simulation (Figure 6b), the surface winds are directed towards the island center, which is a result of the sea breeze. At 10:30 UTC (Figure 6c), small cold pools circumnavigate the island in association with the sea breeze generated boundary layer cumulus clouds. These cold pools have intensified and expanded by 11:30 UTC (Figure 6d). In the 1-km WEAK-EXP simulation at 06:00 UTC (Figure 6e), the background surface winds interact with the downslope winds on the western side of the island. Following sunrise, symmetric upslope flow develops, with the region of convergence occurring on the mountain top, as the slopes warm, with the higher elevations warming more quickly (Figure 6f). A strong cold pool develops on the westward side of the mountain by 10:30 UTC in association with precipitating convection at mountain top. The cold pool propagates down the mountain slope,

Atmos. Chem. Phys. Discuss., https://doi.org/10.5194/acp-2019-399
Manuscript under review for journal Atmos. Chem. Phys.
Discussion started: 20 May 2019

Atmospheric Chemistry and Physics
Open Access
Discussions

causing regions of convergence and convection as it propagates shoreward (Figure 6g), a trend which continues through the next hour (Figure 6h).

The cold pool development and surface flow patterns are different for the STRONG-EXP simulations. The STRONG-EXP flat simulation at 06:00 UTC (Figure 7a), demonstrates the environmental state in this regime before sunrise, where the perturbation potential temperature approximately constant across the domain, and the zonal flow is laminar and from the west (Figure 7a). No clouds have formed as yet at this time. However, after sunrise, clouds start to develop inland, as the strong westerly flow advects the sea breeze eastward, as is evident from the vertically-integrated condensate field (Figure 7b). By 10:30 UTC, cold pools being produced in association with the developing convection are evident. The surface winds have become less westerly due to the interactions with the convectively-generated local mesoscale circulations over and to the lee of the island (Figure 7c). By 11:30 UTC, the cold pools have intensified, expanded, and are exclusively on the lee side of the island (Figure 7d).

The cold pool development is quite different with the introduction of orography. After sunrise in the STRONG-EXP 1 km simulation (9:30 UTC, Figure 7f), the region of reverse flow is associated with convergence, cloud development and precipitation, which subsequently produces cold pools near the top of the mountain (Figure 7f). A strong cold pool is evident expanding towards the shore on the western slope of the island, which interacts with the reverse flow by 10:30 UTC (Figure 7g). The convergence between the outflow boundary and the reverse flow produces additional convection and precipitation (Figure 7g), as is evident with the eastward and westward expansion of integrated condensate contour. By 11:30 UTC (Figure 7h), the region of cold (< 4 K) perturbation potential temperatures has expanded further east in association with the enhanced convective precipitation, and smaller scale circulations are dominating the mountain slope regions. Additionally, clouds and associated cold pools are

Atmos. Chem. Phys. Discuss., https://doi.org/10.5194/acp-2019-399
Manuscript under review for journal Atmos. Chem. Phys.
Discussion started: 20 May 2019

Atmospheric Chemistry and Physics Discussions

evident on the western coast. Clouds are still co-located along the outflow boundary that has now reached the eastern shoreline. It therefore seems that the presence of orography in the STRONG-EXPs initially produces deep convection at mountain top. The cold pool produced in association with this convection converges with the return winds within the wake flow, thereby producing additional convection. The latter continues to develop and move towards the coast with the propagating outflow boundary. This sequence of events is evident in all of the STRONG-EXPs with orography.

Overall, the expansion of clouds towards the shore with increasing orographic height is clearly tied to the development of cold pools from precipitation produced earlier in the day. Convection develops near mountain top and produces one or more cold pools. Because the cold pools are denser than the surrounding air, they flow downslope towards the island shores. The convergence and uplift produced by these shoreward propagating gust fronts initiates new convection. Convection is therefore initially observed at mountain top, but develops closer to the shore later in the day by virtue of these propagating cold pools.

3.3 Precipitation

In this section, we now examine how these changes in convective organization and intensity influence the accumulated precipitation averaged over the land and the entire domain. In figure 8 the accumulated precipitation is demonstrated as a function of island diameter (abscissa), orography (size of symbols) and wind regime (red vs blue). Firstly, it is evident from this figure that regardless of island size and background wind regime more surface precipitation is produced as orography is increased. For example, the 2-km high mountains consistently produce the greatest averaged accumulations. Increasing the topography to 2 kilometers causes increases of 260%, 170%, and 150% in accumulated precipitation over land for the 50-km, 100-

km, and 200-km 2-km high STRONG-EXP simulations, respectively, and increases of 160%, 104%, and 98% for the 50-km, 100-km, and 200-km 2-km WEAK-EXPs, respectively, when compared with the flat, 100km STRONG-EXP simulation. It is interesting that the increases from the 50 km islands to the 100 km islands are larger than those from the 100 km islands to the 200 km islands.

Secondly, the STRONG-EXP simulations consistently produce more precipitation than the WEAK-EXP simulations, regardless of island size or island height, with one exception. The 50 km, flat STRONG-EXP simulation, produces the least amount of precipitation over land of all simulations. This appears to occur because the strong zonal flow advects the convection that initially forms over land off the island, with the result that much of the precipitation occurs over the ocean to the lee of the island. Two factors appear to contribute to the greater precipitation amounts in the STRONG-EXP simulations: (a) the lee vortex formation and reverse flow development in the STRONG-EXPs with orography cause earlier deeper convection as the moisture flux convergence is concentrated near the stagnation point; and (b) the relative humidity is greater in the STRONG-EXP sounding (Robinson et al 2011), which provides more moisture for precipitation.

To further understand how the precipitation field evolves in time with respect to changing island size and orography, we examine the time series of the accumulated precipitation for all the simulations (Figure 9). As the differences between the domain-averaged precipitation amounts were small compared to the land-only averaged precipitation differences, this section focuses on the land-only averaged accumulated precipitation. Increasing the orographic height decreases the time it takes for the initiation and intensification of the precipitation rates. For example, in the 100 km-diameter STRONG-EXP simulation, precipitation begins at 0940 UTC in the flat simulation, but at 0820 UTC in the 2km simulation (Figure 9a). The trend is most noticeable in

Atmos. Chem. Phys. Discuss., https://doi.org/10.5194/acp-2019-399
Manuscript under review for journal Atmos. Chem. Phys.
Discussion started: 20 May 2019

the 50-km diameter STRONG-EXP simulations, where precipitation begins nearly two hours earlier in the 2-km simulation (0750 UTC) than in the flat simulation (0940 UTC). These trends are similar in the WEAK-EXP simulations, although precipitation initiation in all of the WEAK-EXP simulations is delayed when compared with their corresponding STRONG-EXPs. The maximum precipitation rate (mm/10 minutes) increases with increasing orography for all island sizes in both the STRONG-EXP and WEAK-EXP simulations. In summary, precipitation occurs earlier with increasing orography, and the average precipitation rate increases with increasing topography.

Most of the precipitation has stopped accumulating in the STRONG-EXP 1 and 2km-orographic height tests by 12:00 UTC. The 50-km diameter islands have the fastest accumulation (Figure 9a), followed by those of the 100-km and 200-km diameter islands. This appears to be a function of the time it takes for the reverse flow on the lee side of the island to traverse the longer radius in the larger diameter simulations. The 2-km high 100 and 200-km diameter simulations receive similar amounts of precipitation (11.63 & 11.14 mm respectively), but the 100-km diameter island has its greatest accumulation rates from 0900 UTC – 1050 UTC, whereas the 200-km diameter island has its greatest accumulation rates an hour later, from 1000 UTC – 1200 UTC. The trends in the timing of the initiation and most rapid precipitation rates are similar for lower orographic heights, but the magnitudes are smaller, further corroborating that the peak orographic height is a stronger control on the accumulated precipitation than island size in the strong zonal wind regime.

The WEAK-EXP simulations accumulate less precipitation than the STRONG-EXP simulations, and the high precipitation rates do not last as long (Figure 9b). For the tallest mountains, precipitation begins later in the WEAK-EXP simulations than in the STRONG-EXP. For example, in the 50-km diameter island, 2-km high island simulations, precipitation begins to accumulate at 0810 UTC (Figure 9b), compared to 0740 UTC in the STRONG-EXP (Figure 9a), with accumulation rates of 0.8-1.1 mm/10 minutes through 0930 UTC, which taper off to lower rates more quickly than in the STRONG-EXP simulations. A similar pattern exists for the 100-km diameter island. However, the WEAK-EXP 200-km diameter island has a steady accumulation rate from 1000 UTC until 1600 UTC of about .2 mm/10 minutes (.02/minute).

In summary, both the timing of the greatest precipitation rates, as well as the average precipitation accumulations increase monotonically with increasing orographic height, irrespective of island size. When the orographic height is kept constant, then precipitation rates and amounts decrease with increasing island size. These orographic- and diameter-induced differences are driven by the orographic-induced changes to the flow characteristics and the timing of low-level convergence. Convergence takes longer to occur on the 200 km-diameter islands than on the smaller diameter islands, even with the highest topography. This holds true for both the WEAK-EXP and the STRONG-EXP simulations.

3.4 Tracer Redistribution

As described above, all of the model experiments are initialized with 500m deep layers of tracers which are tracked throughout the simulation. No additional release of the tracers occurs. The values shown in the figures corresponding to this analysis are represented as a percentage of the initial tracer amount in the lowest tracer level (0-500m AGL), and thus represent the horizontal and vertical redistribution of the tracers initially located nearest the surface. For example, at the initial time the percentage of this tracer from 0-500 m AGL would be 100%, whereas at higher altitudes, the value would be 0%. However, with the lofting of the tracers in time, the tracer percentage would decrease in the lowest level but increase higher up.

In figure 10, the plan view represents the percent change of the tracer initially located in the lowest level (0-500m AGL) for two layers in the modeled atmosphere, the 0-500 meters AGL level and the 500-1000 meters AGL level. In the STRONG-EXP flat simulations (Figure 10a-f), before sunrise, more than 95% of the original tracer is still resident in the lowest 500 meters, while less than 5% of this tracer is in the 500-1000 m AGL level (Figure 10a,b), indicating the limited amount of vertical mixing that occurs before sunrise. This pattern is similar in the WEAK-EXP simulations (Figure 10g,h). At 09:00 UTC, in the STRONG-EXP simulation, low-level convergence produces tracer lofting which leads to an increase in this tracer at the 500-1000 m AGL level (Figure 10c, d), and as shallow convection initiates, more tracers are lofted from the surface level to the next level (Figure 10e, f). Tracers in the WEAK-EXP are similarly lofted, although the patterns are symmetrical around the island with the weaker zonal flow, in keeping with the flow regimes discussed above. At 09:00 UTC (Figure 10i, j), the transport of the near-surface tracers around the island edges (Figure 10i) through vertical lofting to the 500-1000 m AGL region (Figure 10j) is evidence of the sea-breeze related convergence circumnavigating the island. The continued convergence diminishes the amount of the original tracer in the lowest level with time (Figure 10k, l).

The impacts of orography on the tracer redistribution are demonstrated in Figure 11. In both the STRONG-EXP and WEAK-EXP simulations, tracers are rapidly lifted from the surface at mountain top. This effect is stronger in the STRONG-EXP simulation, where only 5-15% of the original tracer remains in the lowest level at 06:00 UTC (Figure 11a) before sunrise, whereas 30-40% of the original tracer is still evident at the same time (Figure 11g) in the WEAK-EXP. In the STRONG-EXP, up to 70% of the near-surface tracers have been lofted in the lee-vortex downwind of the mountain by 06:00 UTC (Figure 11b). In the WEAK-EXP, a slight downslope wind develops in association with the mountain-valley circulation and is evident early on the

Atmos. Chem. Phys. Discuss., https://doi.org/10.5194/acp-2019-399
Manuscript under review for journal Atmos. Chem. Phys.
Discussion started: 20 May 2019

western portion of the mountain (06:00 UTC, Figure 11g, h). This interaction and subsequent convergence of this flow with the background flow, lofts up to 65% of the original near-surface tracer into the second vertical level. After sunrise, along the coast line, ~70% of the original near-surface tracer gets lofted into the 500-1000 m AGL range (Figure 11i, j), in keeping with the convergence (Fig 3d) and wind flow (Fig 2d) regimes at this point in time. Increasing the orographic height causes the tracers to be lofted higher near mountain top in association with the mountain top convergence, and in the presence of a strong background wind, the tracers are effectively advected into the island wake (Fig 11).

In summary, the redistribution of aerosols in the flat topography cases is closely tied with cloud formation via sea-breeze initiated convection. In the experiments with increased orographic height, the resulting aerosol redistribution occurs due to a combination of the changes to the flow around the islands and the manner in which the location of convection is altered.

4.0 Discussion and Conclusions

In this investigation 24 idealized simulations of tropical islands were conducted in which the island size and orographic height were individually and simultaneously varied under a weak and strong wind regime, in order to determine how the size and topography of an island influences convection, precipitation and aerosol distribution. The simulations utilized three-dimensional circular islands with varying degrees of topographic height. This model setup allows for the development of the complex three-dimensional flow both over and around the islands. Additionally, each simulated island has a realistic land surface of evergreen brush, thus representing the surface flux response to the meteorology. A number of conclusions have been drawn from the analyses of these numerical experiments.

Varying the island diameter has little effect on the overall flow patterns, regardless of the background wind regime. However, enhancing topography, regardless of island size or wind regime, results in substantial changes to the flow around the islands, which in turn impact three primary features: (a) precipitation, (b) convective development and morphology, and (c) aerosol transport. Orography is a stronger control on accumulated precipitation than is island size, with increasing orography producing greater amounts of accumulated precipitation. While a weaker influence, island size also impacts accumulated precipitation, with decreases in the land-averaged precipitation with increasing island size. This decrease in precipitation with increasing island size is different from what has previously been reported by Robinson and Sherwood (2011) who found that increasing island size increased convective vigor and associated precipitation production. In the experiments performed here, precipitation was also found to increase on the lee side of the mountains in the high wind regime in association with the convergence produced by the lee vortices and return flow. This finding also diverges from previous work on this topic (Wang and Sobel, 2017; Nugent et al., 2014). The differences between the results of the simulations conducted here and many of the previous findings is most likely due to the model setup, particularly the domain configuration and the island morphology. Many of the previous simulations were two dimensional, and those that were three dimensional typically used a channel approach, where the y-dimension was typically one tenth of the x-dimension (60 x 600 grid cells); the island was also frequently represented as a strip in the center of the domain that extended the entire meridional extent of the domain. Furthermore, the island was typically modeled using an ocean surface without latent heat fluxes and/or a free-slip boundary. These representations of island morphology do not allow for three dimensional flows around the island, nor for the detailed representation of potentially important surface processes including surface fluxes, surface roughness and the impacts of drag. As the experimental setup used here was intended to mimic the atmospheric conditions of Robinson and Sherwood (2011) as closely as possible, these results suggest that it may be important to fully capture the three-dimensional nature of the flow over and around the island, as well as the role played by surface properties.

Regardless of island diameter or wind regime, convection begins as scattered boundary layer cumulus and grows upscale towards the island center in the flat island simulations. Increasing the island topography changes this behavior. Heightened topography causes convection to initiate predominantly near the center of the islands, quickly become deep convection, and then propagate towards the shorelines. The initiation of convection also varies as a function of wind regime. In the STRONG-EXP simulations, the increasing orography causes lee vortex development, and a strong reverse on-island flow associated with the vortex pair. This wake formation increases surface moisture flux convergence near the stagnation point on the lee side of the island, which leads to earlier and deeper convection. In the WEAK-EXPs, the thermally induced upslope flow creates initial moisture flux convergence near the mountain top, which then initiates deep convection in this location. In both wind regimes with enhanced orography, the expansion of convective activity towards the shoreline throughout the day is tied to the development of cold pools near the island center earlier in the day and the subsequent shoreward propagation of these cold pools. The cold pools play an important role in initiating and sustaining convection as they move towards the ocean. The cold pools do not propagate towards the shore in the flat island cases, and hence this shoreward development of convection is not observed.

The changes in convective organization also affect the horizontal and vertical distribution of aerosols, which were represented using passive tracers in these experiments. In the STRONG-EXP orographic simulations, tracers are lifted from the surface near the mountain tops and advected into the island wake, where ~80% of them remain for much of the rest of the day. This is a function of the lower wind speeds that are characteristic within these wakes (Isoguchi et al., 2010), as well as the reverse flow that develops. In the WEAK-EXP orographic experiments, ~70% of the initial tracer is first lofted from the region of near-surface convergence that occurs as a function of the downslope mountain flow interacting with the background flow. These orographic patterns are different than those which occur in the flat topography simulations, where tracers are entrained into the convection developing after sunrise. While the magnitude of tracer lofting is similar between the WEAK-EXP and STRONG-EXP orographic and flat simulations, the mechanisms are therefore different. In the STRONG-EXP, mechanical forcing via wake and vortex formation plays a predominant role, whereas in the WEAK-EXP the thermally-induced mechanisms of upslope flow arising from diurnal heating dominate. After sunrise, when convection begins, the ability to distinguish the predominant role of the thermal versus mechanical mechanisms becomes difficult to determine.

The results from this study highlight the potentially important role of wake formation in convective organization and aerosol transport. This is keeping with other work that has shown the importance of a hydraulic jump that develops in the lee of the island under conditions of strong environmental flow (Yang et al., 2008). Additionally, the analysis presented here demonstrates that the movement of the cold pools down the mountain slopes assists in causing progressive convective initiation towards the shore as the day develops. This suggests that cold pools and surface interactions may be important in the convective organization, precipitation processes, and aerosol redistribution on mountainous islands. As such, they are worthy of consideration and representation in future island studies.

While the experiments presented here were carefully designed, there are limitations both to the experiment setup and with the analyses. The 1-km horizontal grid spacing, though generally sufficient for convection permitting models, will not fully resolve boundary layer cumulus clouds. The constant vertical spacing of 100 meters is also a limitation, especially close to the surface. The vertical structure was designed to mimic the vertical structure of similar past works. However, enhancing the vertical resolution, particularly near the surface would enhance the representation of the surface processes and cold pools, especially with the imposed orography and surface heterogeneity. Another limitation of these experiments is with the treatment of aerosols. In this experiment, given the focus of the study on aerosol transport, the redistribution of aerosols is represented through the use of passive tracers – they do not absorb or scatter radiation, they do not act as CCN, and they do not get scavenged by precipitation. Considering that cloud formation and development is an important mechanism in tracer transport, the lack of accountability in the cloud processing of aerosols means we are potentially missing aerosol loss and production processes. By not including radiatively active aerosols, we are also not accounting for both direct and semi-direct effects, which could influence the mesoscale circulation (Grant et al., 2014; Lee, 2012). The next step in this research is to perform a similar suite of experiments using aerosols that are fully microphysically and radiatively active. Additionally, by not including the Corolis effect, the latitudinal shifts in the timing of the land-sea breeze circulation and the potential interactions with the mountain-breeze circulation (Rotunno, 2983), are not included in this experiment. Finally, while we have tested two different environmental regimes, countless others are observed in the tropics, and the study could be expanded to include additional environments.

In summary, in spite of the study limitations, this research clearly demonstrates the importance of orography and the resulting three-dimensional flow around tropical islands in determining the initiation and amounts of precipitation, the convective organization, and aerosol redistribution. Firstly, increasing island orographic height consistently increased accumulated precipitation on the islands, regardless of island size or wind regime. For a 100-km diameter island, increasing orography from flat to 2 km increases the accumulated precipitation by 170% and encourages the earlier onset of precipitation. Secondly, by representing three-dimensional flow, an interactive surface and the full diurnal cycle, the impacts of both the mountain and sea-breeze circulations on convective organization have been shown. With a weak zonal flow, the increasing topography increases the convergence at mountain top, which occurs as a function of diurnal heating. Under strong zonal flow, the formation of a wake, lee vortices and a reverse flow increase convergence on the lee side of the mountain, which leads to earlier development of deep convection downwind of the mountain top. With both flow regimes, enhanced topography results in the shoreward expansion of convection. This change in convective morphology occurs as a function of cold pools, which form, propagate down the island mountain slopes, and initiate and maintain convection as they progress towards shore. Finally, the aerosol redistribution is closely tied to the development of convection. In the flat topography cases, aerosol redistribution is driven by cloud formation associated with the sea breeze. In the enhanced topography cases, the tracers are transported away from the mountain tops and their fates are more strongly dependent on the specific circulations developing in association with the background wind regime. Examining, understanding, and quantifying these relationships at these fine scales is imperative if the community intends to create parameterizations that represent the impacts of island size and orography on precipitation, convective organization and aerosol transport.

Author Contributions

Stacey Kawecki is the lead author and performed the experiment and wrote the manuscript. Susan van den Heever guided the research and analysis and extensively contributed to the manuscript.

Acknowledgements

This work was supported by the Office of Naval Research under Grant N00014-16-1-2040 with project titled, "*Advancing Littoral Zone Aerosol Prediction via Holistic Studies in Regime-Dependent Flows"*. The authors are grateful for conversations with Kristen Rasmussen on mountain flow regimes.

References

Adler, R.F., and Mack, R., A. Thunderstorm cloud top dynamics as inferred from satellite observations and a cloud top parcel model. Journal of the atmospheric sciences, 43.18, 1945-1960, 1986.

Alexander, M. J., and Grimsdell, A.,W. Seasonal cycle of orographic gravity wave occurrence above small islands in the Southern Hemisphere: Implications for effects on the general circulation. Journal of Geophysical Research: Atmospheres 118.20, 11-589, 2013.

Baker, R. D., Lynn, B. H., Boon, A., Tao, W. K., and Simpson, J. The influence of soil moisture, coastline curvature, and land-breeze circulations on sea-breeze-initiated precipitation. Journal of Hydrometeorology, 2.2, 193-211, 2001.

Birch, C. E., Roberts, M. J., Garcia-Carreras, L., Ackerly, D., Reeder, M. J., Lock, A. P., and Schiemann, R. Sea-breeze dynamics and convection initiation: The influence of convective parameterization in weather and climate model biases. Journal of Climate, 28.20, 8093-8108, 2015.

Boucher, O., et al. Clouds and aerosols. Climate change 2013: the physical science basis. Contribution of Working Group I to the Fifth Assessment Report of the Intergovernmental Panel on Climate Change. Cambridge University Press, 571-657, 2013.

Broccoli, A. J., and Manabe, S. The effects of orography on midlatitude Northern Hemisphere dry climates. Journal of Climate 5.11, 1181-1201, 1992.

Campetella, C. M., and Vera, C. S. The influence of the Andes mountains on the South American low-level flow. Geophysical Research Letters 29.17, 2002.

Chen, Y., and Wang, J. Diurnal variation of surface thermodynamic fields on the island of Hawaii. Monthly weather review 122.9, 2125-2138, 1994.

Choi, H. and Hong, S. An updated subgrid orographic parameterization for global atmospheric forecast models. Journal of Geophysical Research: Atmospheres 120.24, 12445-12457, 2015.

Corfidi, S. F., Cold pools and MCS propagation: Forecasting the motion of downwind-developing MCSs. Weather and forecasting, 18.6, 997-1017, 2003.

Atmos. Chem. Phys. Discuss., https://doi.org/10.5194/acp-2019-399
Manuscript under review for journal Atmos. Chem. Phys.
Discussion started: 20 May 2019

Emanuel, K. A. Atmospheric convection. Oxford University Press on Demand, 1994.

Epifanio, C. C., and Rotunno, R. The dynamics of orographic wake formation in flows with upstream blocking. Journal of the atmospheric sciences 62.9, 3127-3150, 2005.

Etling, D. On atmospheric vortex streets in the wake of large islands. Meteorology and Atmospheric Physics 41.3, 157-164, 1989.

Fan, J., Rosenfeld, D., Yang, Y., Zhao, C., Leung, L. R., and Li, Z. Substantial contribution of anthropogenic air pollution to catastrophic floods in Southwest China. Geophysical Research Letters 42.14, 6066-6075, 2015.

Fan, Jiwen, et al. "Review of aerosol–cloud interactions: mechanisms, significance, and challenges." *Journal of the Atmospheric Sciences* 73.11 (2016): 4221-4252.

Glover, R.W. Influence of spatial resolution and treatment of orography on GCM estimates of the surface mass balance of the Greenland Ice Sheet. Journal of Climate 12.2, 551-563, 1999.

Grant, L. D., and van den Heever, S. C. Aerosol-cloud-land surface interactions within tropical sea breeze convection. Journal of Geophysical Research: Atmospheres, 119.13, 8340-8361, 2014.

Hassim, M. E. E., Lane, T. P., and Grabowski, W. W. The diurnal cycle of rainfall over New Guinea in convection-permitting WRF simulations. Atmospheric Chemistry & Physics Discussions, 16.1, 2016.

Hill, G. E. Factors controlling the size and spacing of cumulus clouds as revealed by numerical experiments. Journal of the Atmospheric Sciences, 31.3, 646-673, 1974.

Holton, J. R., and Hakim, G. J. An introduction to dynamic meteorology. Vol. 88. Academic press, 2012.

Houze, R.A. Orographic effects on precipitating clouds. Reviews of Geophysics, 50.1, 2012.

Isoguchi, O., Shimada, M., and Kawamura, H. Characteristics of ocean surface winds in the lee of an isolated island observed by synthetic aperture radar. Monthly Weather Review, 139.6, 1744-176, 2010.

Kanitz, T., Ansmann, A., Foth, A., Seifert, P., Wandinger, U., Engelmann, R., Baars, H., Althausen, D., Casiccia, C., and Zamorano, F. Surface matters: limitations of CALIPSO V3 aerosol typing in coastal regions. Atmospheric Measurement Techniques, 7.7, 2061-2072, 2014.

Lee, S. S. Effect of aerosol on circulations and precipitation in deep convective clouds. Journal of the Atmospheric Sciences, 69.6, 1957-1974, 2012.

Mahrer, Y. and Pielke, R. A. The effects of topography on sea and land breezes in a two-dimensional numerical model. Monthly weather review, 105.9, 1151-1162, 1977.

McFarlane, N. A. The effect of orographically excited gravity wave drag on the general circulation of the lower stratosphere and troposphere. Journal of the atmospheric sciences, 44.14, 1775-1800, 1987.

McGranahan, G., Balk, D., and Anderson, B. The rising tide: assessing the risks of climate change and human settlements in low elevation coastal zones. Environment and urbanization, 19.1, 17-37, 2007.

Minder, J. R., Smith, R. B., and Nugent, A. D. The dynamics of ascent-forced orographic convection in the tropics: Results from Dominica. Journal of the Atmospheric Sciences, 70.12, 4067-4088, 2013.

Neale, R. and Slingo, J. The Maritime Continent and its role in the global climate: A GCM study. Journal of Climate,16.5, 834-848, 2003.

Neumann, B., Vafeidis, A. T., Zimmermann, J., and Nicholls, R. J. Future coastal population growth and exposure to sea-level rise and coastal flooding-a global assessment. PloS one, 10.3, e0118571, 2015.

Nugent, A. D., Smith, R. B., and Minder, J. R. Wind speed control of tropical orographic convection. Journal of the Atmospheric Sciences, 71.7, 2695-2712, 2014.

Pielke, R. A. A three-dimensional numerical model of the sea breezes over south Florida. Monthly weather review, 102.2, 115-139, 1974.

Pielke, R. A., Cotton, W. R., Walko, R. E. A., Tremback, C. J., Lyons, W. A., Grasso, L. D., Nicholls, M. E., Moran, M. D., Wesley, D. A., Lee, T. J., and Copeland, J. H. A comprehensive meteorological modeling system—RAMS. Meteorology and atmospheric Physics, 49.1-4, 69-91, 1992.

Rasmussen, K. L., and Houze, R. A. Convective initiation near the Andes in subtropical South America. Monthly Weather Review,144.6, 2351-2374, 2016.

Reid, J. S., Hyer, E. J., Johnson, R. S., Holben, B. N., Yokelson, R. J., Zhang, J., Campbell, J. R., Christopher, S. A., Di Girolamo, L., Giglio, L., and Holz, R. E. Observing and understanding the Southeast Asian aerosol system by remote sensing: An initial review and analysis for the Seven Southeast Asian Studies (7SEAS) program. Atmospheric Research, 122, 403-468, 2013.

Robinson, F. J., Sherwood, S. C., Gerstle, D., Liu, C., and Kirshbaum, D. J. Exploring the land–ocean contrast in convective vigor using islands. Journal of the Atmospheric Sciences, 68.3, 602-618, 2011.

Rotunno, R. On the linear theory of the land and sea breeze. Journal of the Atmospheric Sciences, 40.8, 1999-2009, 1983.

Rotunno, R., Grubišić, V., and Smolarkiewicz, P. K. Vorticity and potential vorticity in mountain wakes. Journal of the atmospheric sciences, 56.16, 2796-2810, 1999.

Saleeby, S. M., and Cotton, W. R. A large-droplet mode and prognostic number concentration of cloud droplets in the Colorado State University Regional Atmospheric Modeling System (RAMS). Part I: Module descriptions and supercell test simulations. Journal of Applied Meteorology, 43.1, 182-195, 2004.

Atmos. Chem. Phys. Discuss., https://doi.org/10.5194/acp-2019-399
Manuscript under review for journal Atmos. Chem. Phys.
Discussion started: 20 May 2019

Saleeby, S. M., and Cotton, W. R. A binned approach to cloud-droplet riming implemented in a bulk microphysics model. Journal of Applied Meteorology and Climatology, 47.2, 694-703, 2008.

Saleeby, S. M., and van den Heever, S. C. Developments in the CSU-RAMS aerosol model: Emissions, nucleation, regeneration, deposition, and radiation. Journal of Applied Meteorology and Climatology, 52.12, 2601-2622, 2013.

Sherwood, S.C., Minnis, P., and McGill, M. Deep convective cloud-top heights and their thermodynamic control during CRYSTAL-FACE. Journal of Geophysical Research: Atmospheres, 109.D20, 2004.

Smith, R. B., and Grubišić, V. Aerial observations of Hawaii's wake. Journal of the atmospheric sciences, 50.22, 3728-3750, 1993.

Smith, R. B., Minder, J. R., Nugent, A. D., Storelvmo, T., Kirshbaum, D. J., Warren, R., Lareau, N., Palany, P., James, A., and French, J. Orographic precipitation in the tropics: The Dominica Experiment. Bulletin of the American Meteorological Society, 93.10, 1567-1579, 2012.

Smolarkiewicz, P. K., and Rotunno, R. Low Froude number flow past three-dimensional obstacles. Part I: Baroclinically generated lee vortices. Journal of the Atmospheric Sciences, 46.8, 1154-1164, 1989.

Tao, W. K., Chen, J. P., Li, Z., Wang, C., and Zhang, C. Impact of aerosols on convective clouds and precipitation. Reviews of Geophysics, 50.2, 2012.

Walko, R. L., Band, L. E., Baron, J., Kittel, T. G., Lammers, R., Lee, T. J., Ojima, D., Pielke Sr, R. A., Taylor, C., Tague, C., and Tremback, C. J. Coupled atmosphere–biophysics–hydrology models for environmental modeling. Journal of applied meteorology, 39.6, 931-944, 2000.

Wang, C. C., and Kirshbaum, D. J. Thermally forced convection over a mountainous tropical island. Journal of the Atmospheric Sciences, 72.6, 2484-2506, 2015.

Wang, C. C., and Kirshbaum, D. J. Idealized simulations of sea breezes over mountainous islands. Quarterly Journal of the Royal Meteorological Society, 143.704, 1657-1669, 2017.

Wang, J., Ge, C., Yang, Z., Hyer, E. J., Reid, J. S., Chew, B. N., Mahmud, M., Zhang, Y., and Zhang, M. Mesoscale modeling of smoke transport over the Southeast Asian Maritime Continent: Interplay of sea breeze, trade wind, typhoon, and topography. Atmospheric Research, 122, 486-503, 2013.

Wang, S., and Sobel, A. H. Factors controlling rain on small tropical islands: Diurnal cycle, large-scale wind speed, and topography. Journal of the Atmospheric Sciences, 74.11, 3515-3532, 2017.

Yang, G. Y., and Slingo, J. The diurnal cycle in the tropics. Monthly Weather Review, 129.4, 784-801, 2001.

Yuter, S. E., and Houze Jr., R. A. Three-dimensional kinematic and microphysical evolution of Florida cumulonimbus. Part II: Frequency distributions of vertical velocity, reflectivity, and differential reflectivity. Monthly weather review, 123.7, 1941-1963, 1995.

Atmos. Chem. Phys. Discuss., https://doi.org/10.5194/acp-2019-399
Manuscript under review for journal Atmos. Chem. Phys.
Discussion started: 20 May 2019

Table 1: Regional Atmospheric Modeling System (RAMS) Configuration

Domain size:Nx,Ny,Nz	[100,200,400],[100,200,400],200
Δx, Δy, Δz, Δt	1km, 1km, 100m, 1 second
Boundary conditions	Initialized from soundings (Robinson et al, 2011) Cyclic
Microphysics	2 moment bulk scheme (Saleeby and Cotton 2004)
SW & LW radiation, Δt	Harrington 2-stream, 60 seconds
Surface model	LEAF3 (Walko et al, 2000)
Dynamics	Fully compressible; No Coriolis Force
Aerosols	Passive Tracers, near surface [0-500m above ground level; mixing ratio of 1 kg/kg]

Table 2: Experimental Set Up: For each island diameter (top row), simulations are run for increasing peak orographic heights. This set of twelve simulations is run for a strong zonal wind regime (STRONG-EXP simulations) and a weak zonal wind regime (WEAK-EXP simulations).

50 km	**100 km**	**200 km**
Flat	Flat	Flat
500 meters	500 meters	500 meters
1 km	1 km	1 km
2 km	2 km	2km

Atmos. Chem. Phys. Discuss., https://doi.org/10.5194/acp-2019-399
Manuscript under review for journal Atmos. Chem. Phys.
Discussion started: 20 May 2019

Figures

Figure 1

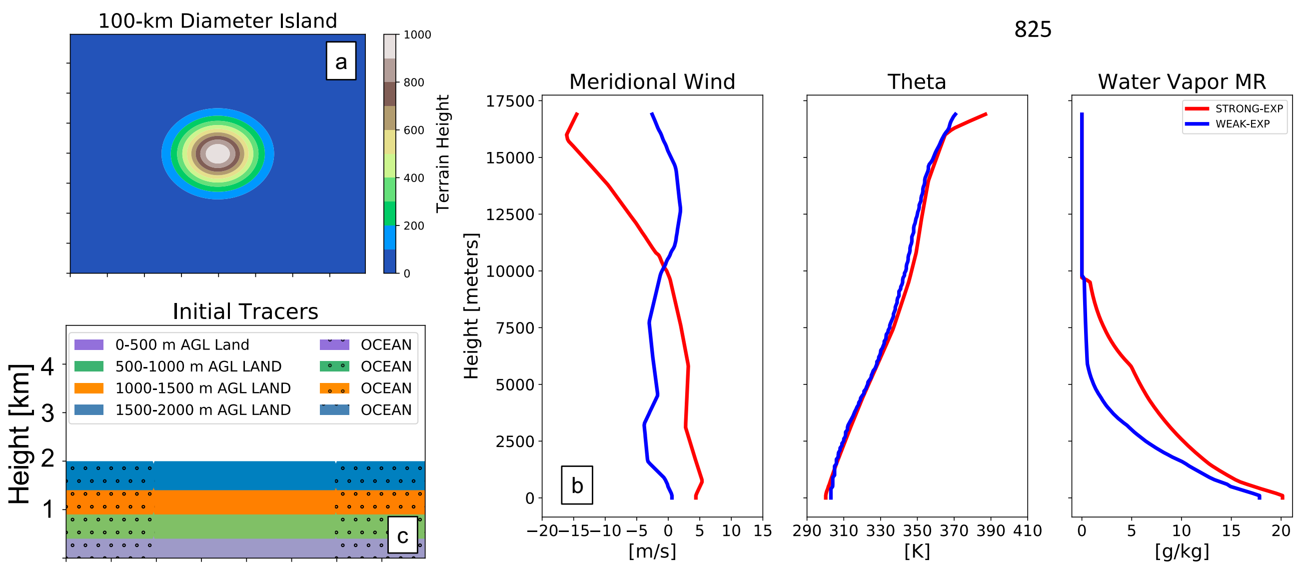

Figure 1: Schematic of the experimental design: (a) the horizontal domain and the varying topographic height of the 100-km diameter island; (b) the vertical profiles of zonal wind components, potential temperature, and water vapor mixing ratio for the STRONG-EXP (red) and WEAK-EXP (blue) experiments; (c) the vertical tracer distribution over the 100 km diameter flat island, where hashing indicates tracers released over ocean.

Atmos. Chem. Phys. Discuss., https://doi.org/10.5194/acp-2019-399
Manuscript under review for journal Atmos. Chem. Phys.
Discussion started: 20 May 2019

Atmospheric Chemistry and Physics Discussions

833 **Figure 2**

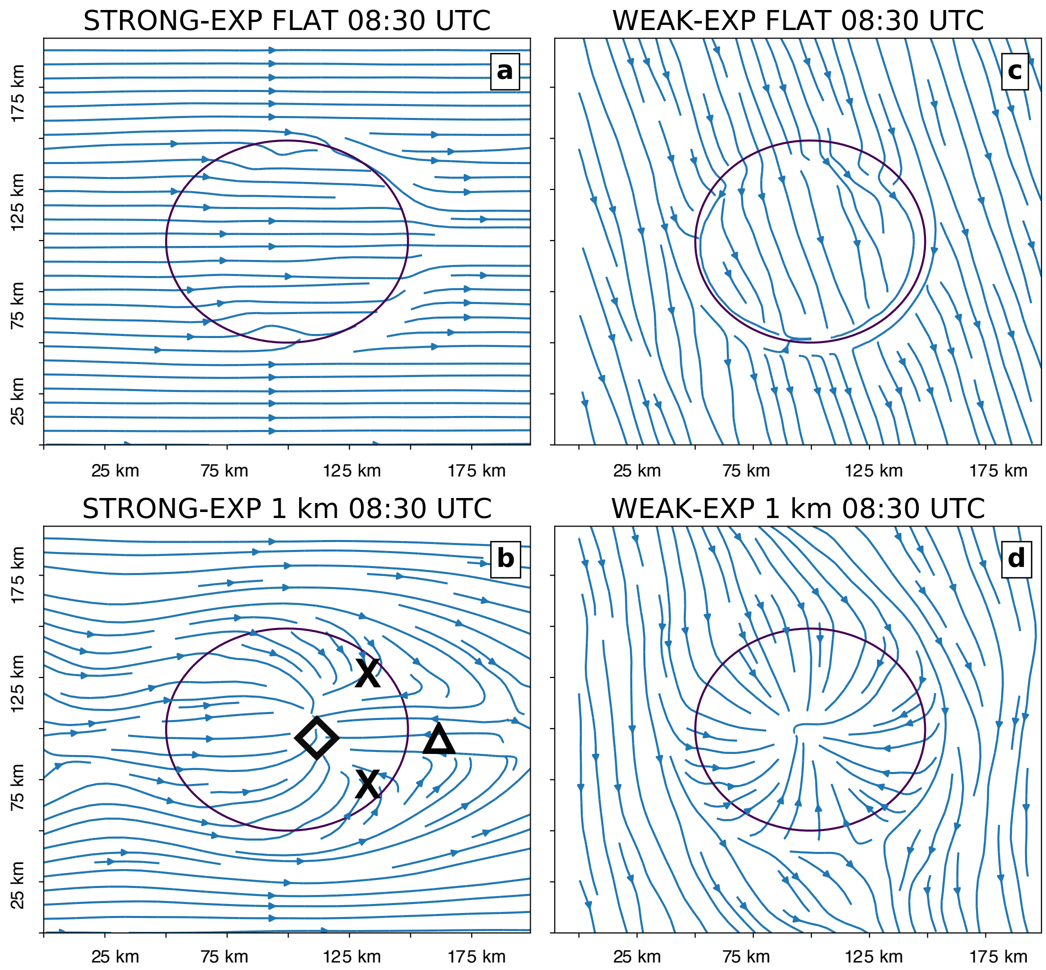

834

835 **Figure 2:** Surface streamlines (~ 50 meters) for 100-km diameter island simulations at 08:30
836 UTC, for the STRONG-EXP (a and b) and the WEAK-EXP (c and d), flat (a and c) and 1-km
837 height (b and d) simulations. The black diamond indicates the stagnation point, the black "x"
838 denote the placement of lee vortices and the black triangle demonstrates where the reverse flow
839 occurs.

840

Atmos. Chem. Phys. Discuss., https://doi.org/10.5194/acp-2019-399
Manuscript under review for journal Atmos. Chem. Phys.
Discussion started: 20 May 2019

Atmospheric Chemistry and Physics
Discussions

Figure 3

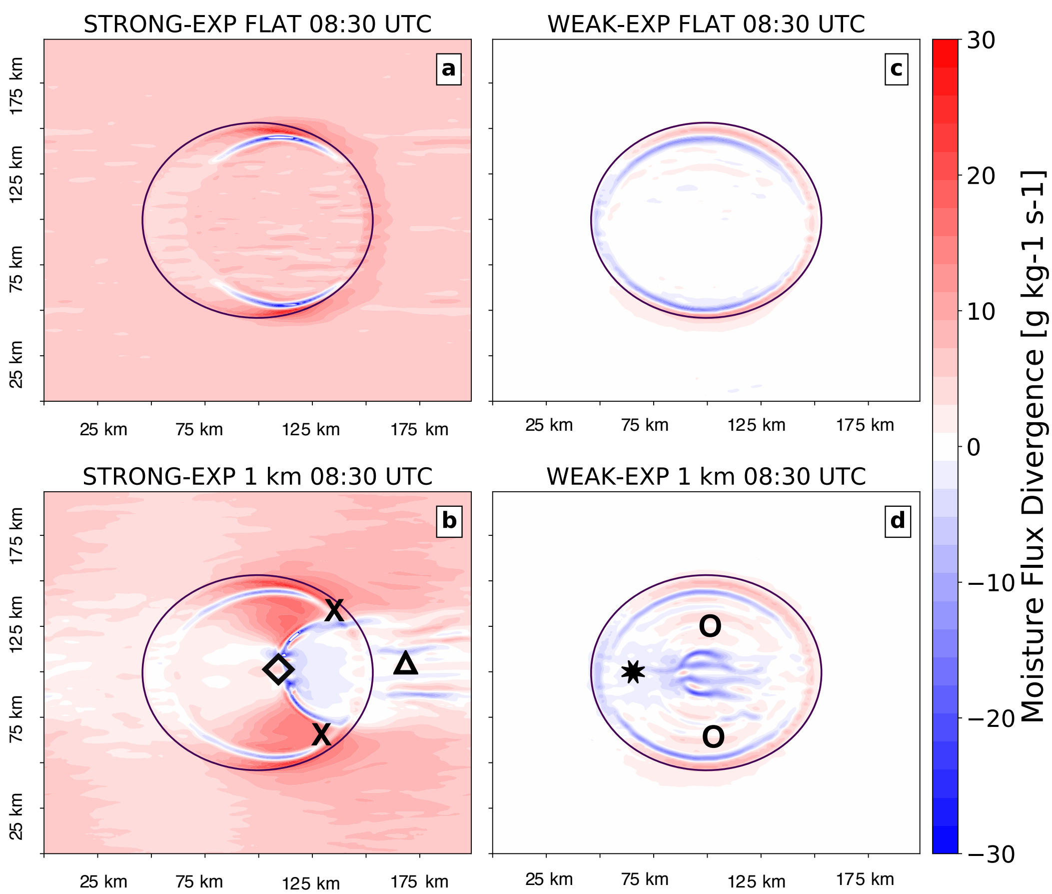

Figure 3: Surface moisture flux divergence for 100-km diameter island simulations at 08:30 UTC, for the STRONG-EXP (a&b) and the WEAK-EXP (c&d), flat (a&c) and 1-km height (b&d) simulations. The black X's, diamond, and triangle are the same as figure 2. The black circles indicate regions of upslope flow and moisture flux divergence, whereas the black star indicates a region of moisture flux convergence.

Figure 4

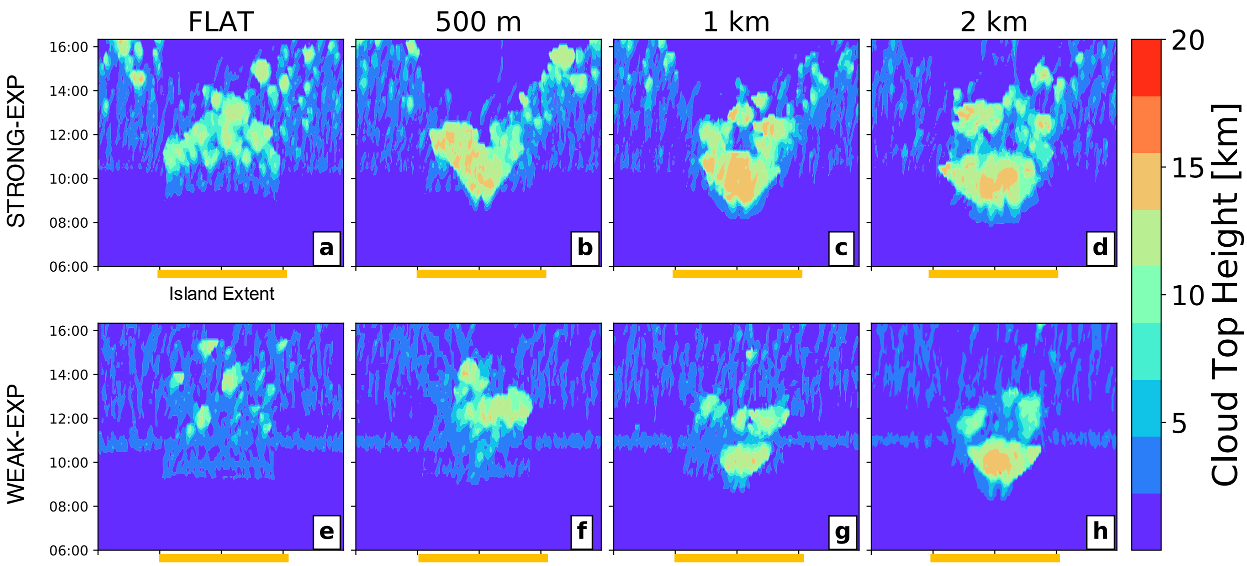

Figure 4: Hovmöller plots of latitudally-averaged cloud top height for the 100km island diameter simulations, with STRONG-EXP simulations (a-d) and WEAK-EXP simulations (e-h), with orographic height increasing from left to right.

Figure 5

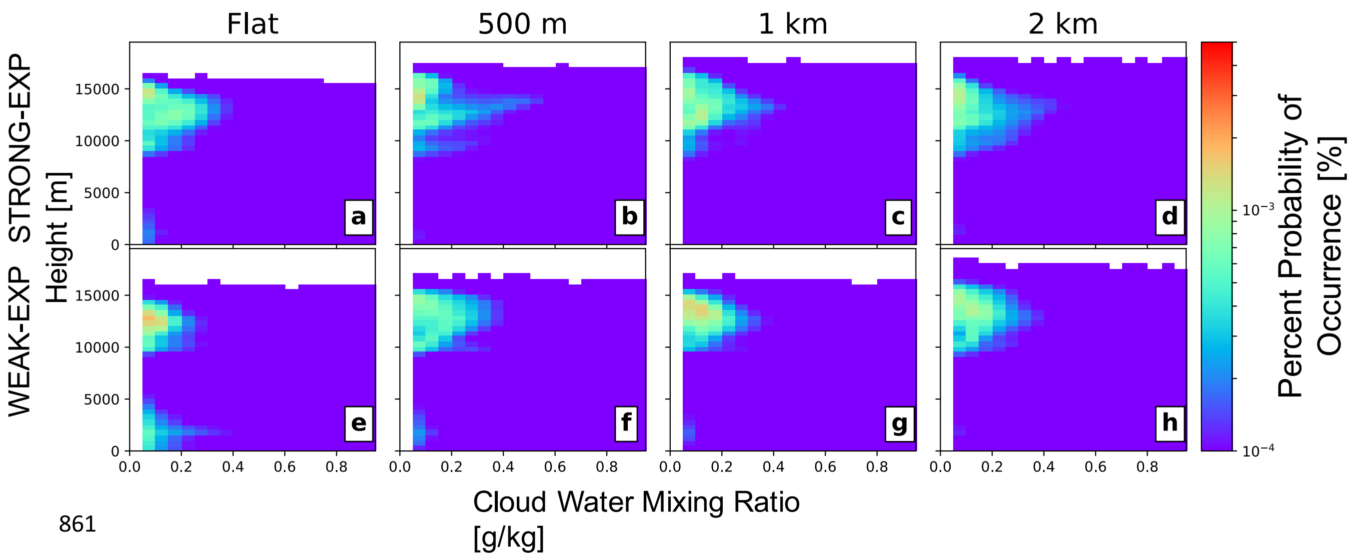

Figure 5: CFADs of cloud water mixing ratio [g/kg] for the STRONG-EXP simulations (a-d) and the WEAK-EXP simulations (e-h), with orographic height increasing from left to right. Shading is the percent probability of occurrence.

Figure 6

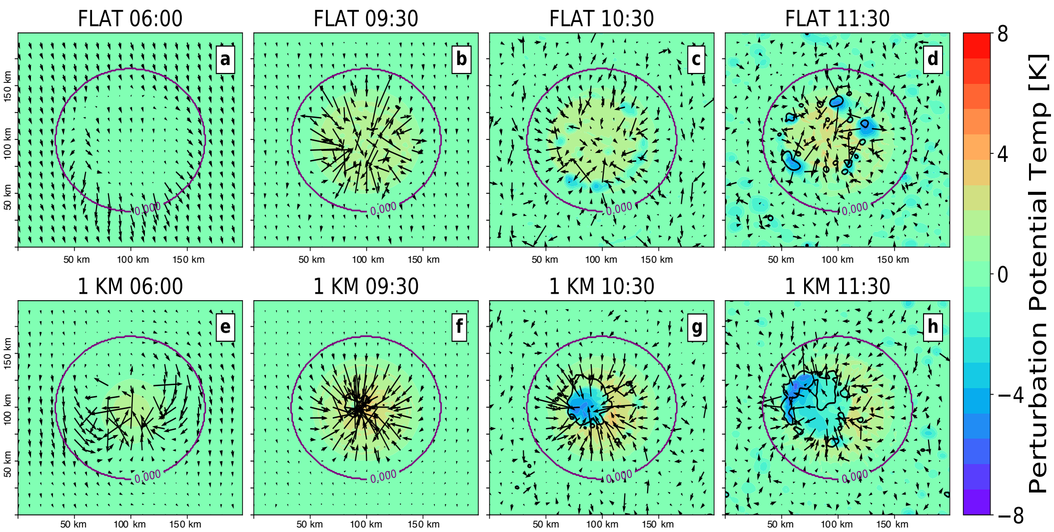

Figure 6: Surface potential temperature perturbation (K, colored contours), surface winds (arrows; m/s), and the 20 g/kg integrated condensate mixing ratio isoline (black contour) for the 100-km WEAK-EXP simulations, showing the time dependent evolution of convective features for the FLAT simulation (a-d) and the 1-km Height simulation (e-h).

Figure 7

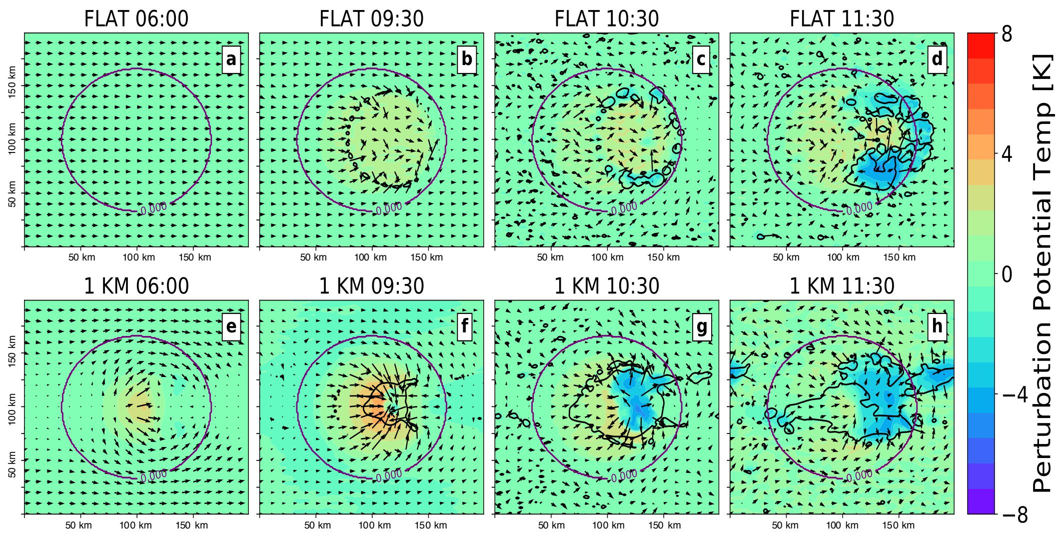

Figure 7: Same as Figure 8, except for the WEAK-EXP 100-km diameter islands.

Figure 8

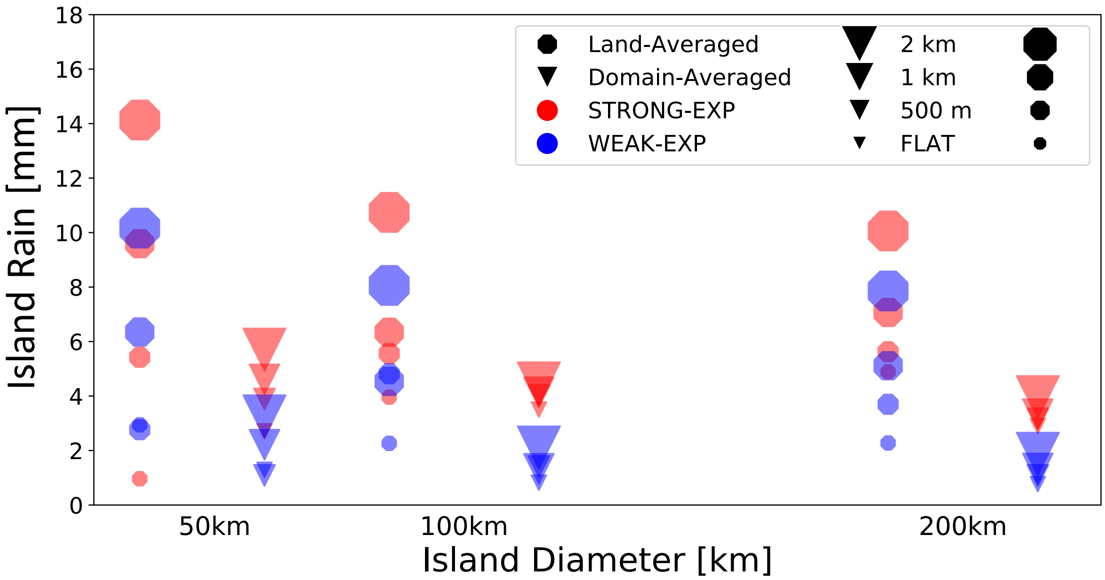

Figure 8: Scatter plot showing the area-averaged accumulated precipitation for each simulation as a function of island size. Triangles indicate that the averages are performed over the entire domain, whereas octagons indicate precipitation is averaged over land only. Blue markers indicate the STRONG-EXP simulations, and red markers indicate the WEAK-EXP simulations.

Atmos. Chem. Phys. Discuss., https://doi.org/10.5194/acp-2019-399
Manuscript under review for journal Atmos. Chem. Phys.
Discussion started: 20 May 2019

Figure 9

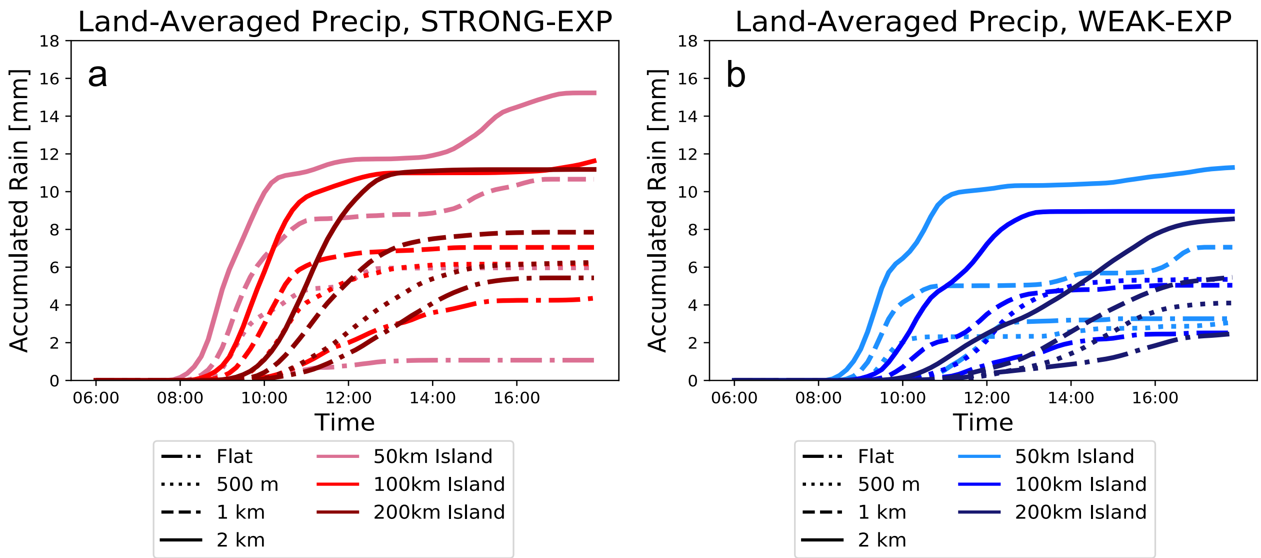

Figure 9: Time series of accumulated precipitation, averaged over land, for (a) the STRONG-EXP and (b) the WEAK-EXP simulations.

Atmos. Chem. Phys. Discuss., https://doi.org/10.5194/acp-2019-399
Manuscript under review for journal Atmos. Chem. Phys.
Discussion started: 20 May 2019

918 **Figure 10**

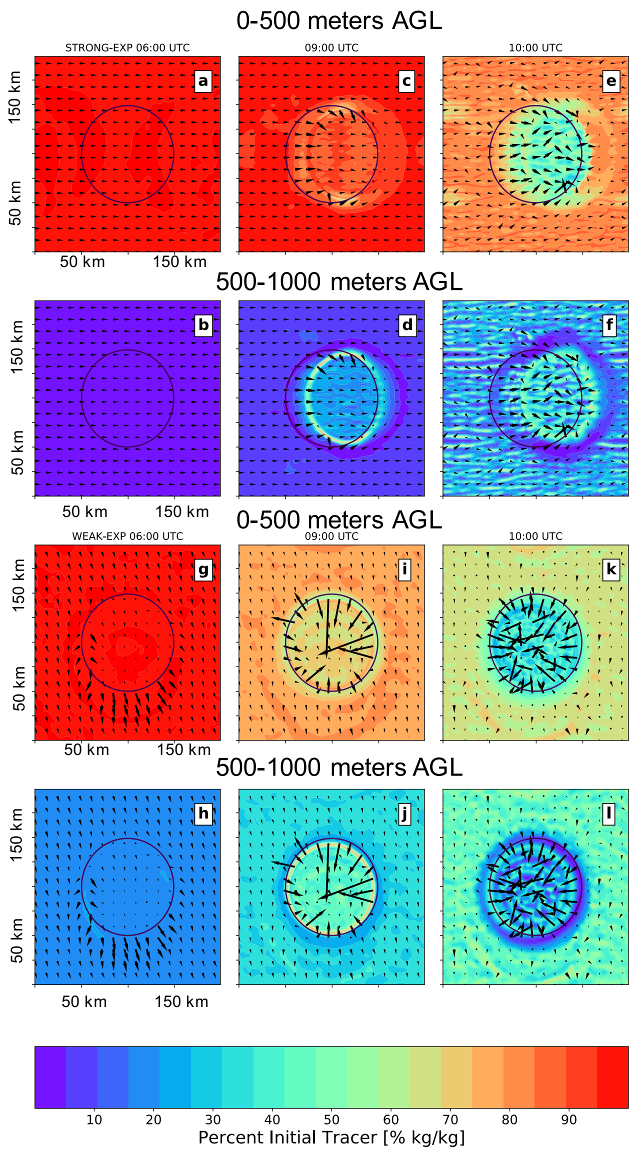

919

920 **Figure 10:** The temporal evolution of the percentage of the initial tracers (colored shading, %

921 kg/kg**)** located in the 0-500m level AGL found at 0-500m AGL (top row) and at 500-1000m

922 AGL (bottom row), for the 100-km, flat, STRONG-EXP (a-f) and WEAK-EXP (g-l).. Shown are

Atmos. Chem. Phys. Discuss., https://doi.org/10.5194/acp-2019-399
Manuscript under review for journal Atmos. Chem. Phys.
Discussion started: 20 May 2019

plans views at the respective heights (0-500m in the top row, 500-1000m in the bottom row). Near surface winds are black wind vectors (m/s).

926 **Figure 11**

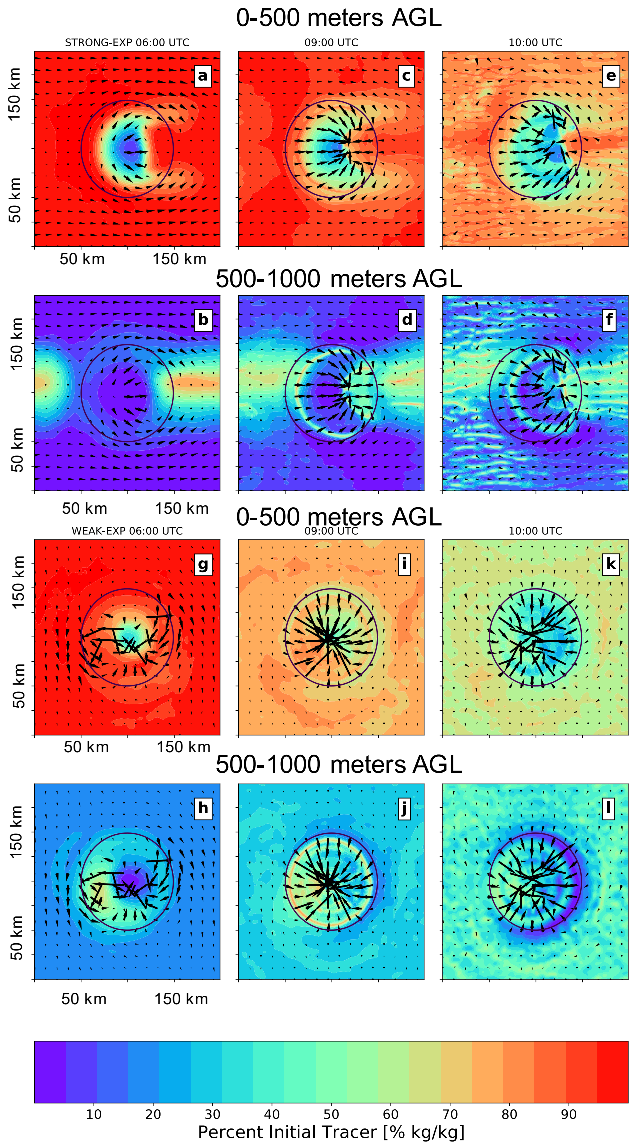

927

928

929 **Figure 11:** Same as Figure 10, except for 100-km diameter, 1-km Height simulations.